# RF Characterization of a Photocurable PEDOT:PSS:PEGDA Conductive Biomaterial for 3D-Printing Implantable Antennas

Balaji Dontha, *Student Member, IEEE*, Mohammad Moulod, Sharolyn Balbaugh, David Hoelzle, *Member, IEEE*, Jinghua Li, *Member IEEE*, Félix A. Miranda, *Fellow*, *IEEE*, and Asimina Kiourti, *Senior Member, IEEE*

***Abstract*—In this work, we a demonstrate photocurable PEDOT:PSS:PEGDA biomaterial as a promising candidate for 3D-printing implantable antennas intracorporeally. Previous work has demonstrated the feasibility of a robotic probe to 3D-print biological tissues via a minor incision. This same probe could also 3D-print implantable antennas as long as a suitable conductive material is identified in terms of conductivity, printability, biocompatibility, and ability to cure at room/body temperature for safety purposes. We assess the frequency-dependent conductivity of this biomaterial and explore the Radio-Frequency (RF) performance of resulting antennas operating in free-space and inside tissue-emulating phantoms. Results show that PEDOT:PSS biomaterials with 21% and 30% PEGDA concentration exhibit a conductivity of ~$10^4$ S/m up to 5 GHz, suitable for wireless implants. Comparing the two, 21% PEGDA content exhibits poorer curing abilities, while 30% PEGDA exhibits slightly lower conductivity. Measurements for 2.4 GHz free-space dipoles conducted in an anechoic chamber reveal only ~0.8 dB and ~1 dB lower gain for PEDOT:PSS:21%PEGDA and PEDOT:PSS:30%PEGDA biomaterial, respectively, as compared to their copper counterpart. For a 5 mm-deep implanted patch antenna, these two biomaterials exhibit 3.05 dB and 3.84 dB higher transmission loss than copper, respectively. If deemed necessary, this performance degradation can be overcome by increasing the overall antenna size since the printing process is now minimally invasive and miniaturization requirements can be relaxed.**

***Index Terms*—3D-printing, biomaterial, conductivity, implantable antenna, RF performance.**

## I. Introduction

Wireless implants functionalized with antennas are becoming increasingly appealing for various diagnostic, therapeutic, and monitoring applications such as pacemakers and cardioverter defibrillators [1-2], intra-cranial pressure monitors [3-4], neuro-sensors/stimulators [5-7], body temperature sensors [8], gastric stimulators [9], and blood glucose monitors [10,11], among others. Traditional surgeries to implant these devices are highly invasive, require prolonged recovery time, and often lead to post-operative complications [12-14]. Though electronics can be miniaturized and potentially embedded inside the body by means of injection [15], there are fundamental electromagnetic limits as to how small the implantable antenna can be while still maintaining adequate Radio-Frequency (RF) performance [16-18]. For example, a volumetric antenna reduction by 65% results in a 19% reduction in maximum gain and 80% increase in the maximum 1g-averaged Specific Absorption Rate (SAR) [19].

Minimally invasive, intracorporeal (meaning inside the body) 3D-printing of implantable antennas shows great promise. In intracorporeal 3D printing, a small diameter (order of 8 mm) probe enters a keyhole surgery site and delivers (prints) material in a specific pattern. Multiple probes, or material exchanges, can be used to create multi-material antennas. Besides the safety benefits associated with this approach, a special advantage is that antenna miniaturization requirements can now be relaxed without altering the size of the incision [20]. In [21], authors printed an interstitial antenna using a coaxial applicator that heats a conductive polymer at 40° C and cures it in 10 sec. However, the resulting conductivity was poor (9.09 S/m), while the need to apply heat inside the body is undesirable for safety reasons.

In a major step forward, we envision intracorporeal 3D-printing of implantable antennas using high-conductivity materials that are delivered and cured at room/body temperature. Our approach utilizes a robotic delivery probe that has been previously reported for 3D-printing biological tissues intracorporeally [22]. That is, the printing of lossy dielectrics has already been demonstrated [22], but suitable conductive inks have yet to be explored. Here, the term 'suitable' refers to inks that: (a) exhibit conductivity of at least $10^4$ S/m as deemed necessary for maintaining adequate RF performance [23], (b) are curable at room/body temperature to ensure patient safety, (c) are biocompatible, and (d) can be mechanically delivered by the printer.

In this work, we report Poly-3,4-Ethylene Di-Oxy Thiophene (PEDOT) Polystyrene Sulfonate (PSS) Poly-Ethylene Glycol Di-Acrylate (PEGDA), a polymer-based conductive biomaterial cured using a 365 nm ultraviolet (UV) light, as a promising candidate for the intracorporeal fabrication of antennas. We report measurements of conductivity up to 6 GHz, which covers some of the most important bands for wireless implants [24]. We also fabricate and assess the RF performance of free-space dipole and implantable patch antennas at 2.4 GHz. A comparison with other conductive polymers used for biomedical applications in the literature (see Table I) shows improved conductivity, curing, and safety (temperature and biocompatibility) performance for the proposed PEDOT:PSS:PEGDA biomaterial [25-29].

Manuscript received March 04, 2023, revised December XX, 2023. This work was supported in part by an Ohio State University President's Accelerator Award and NSF IIP 1919204.

B. Dontha, M. Moulod, D. Hoelzle, J. Li and A. Kiourti are with The Ohio State University, Columbus, OH, 43221, USA (e-mail: {dontha.1, moulod.1, balbaugh.9, hoelzle.1, li.11017, kiourti.1}@osu.edu).

F. A. Miranda is with the NASA Glenn Research Center, Cleveland, OH 44135 USA.

TABLE I
COMPARISON OF CONDUCTIVE POLYMERS

| Material | Conductivity | Annealing Temperature | Curing Time | Biocompatible | Frequency of Operation | Application | Ref |
|---|---|---|---|---|---|---|---|
| PEDOT:PSS | $2x10^3$ S/m | 60°C | 24 H | Not Tested | 1 kHz | In-vivo recording of neural brain activity | [25] |
| Nafion/PEDOT | 500 S/m | 30 -70°C | 0.5 to 4 H | Yes | DC | Wearable sensors | [26] |
| PEG/PEI/GNPs | $3.85x10^4$– $5.33x10^4$ S/m | RT*-450°C | NA | No | DC | Bio-electronics | [27] |
| PLA/GNPs | 0.98 S/m | 60°C | NA | Yes | 8-12 GHz | EMI shielding | [28] |
| HPC/Fe3O4-GNPs | 85-580 S/m | 20-180°C | 0.16 H | No | 8.2-12.4 GHz | EMI | [29] |
| PEDOT:PSS: PEGDA (this work) | ~$2x10^4$ S/m | RT | 0.016 H | Yes | 0.1-5 GHz | Implantable antennas | -- |

For this proof-of-concept study, we print PEDOT:PSS:PEGDA on off-the-shelf dielectric substrates with 3D-printing being conducted outside the tissue environment. Printing of dielectrics can be readily performed using the materials and methods reported in [22], while printing directly inside biological tissues is a topic of future research. In this work, the objective is to obtain a comprehensive understanding of the PEDOT:PSS:PEGDA electromagnetic behavior, with the ultimate goal of 3D-printing fully-functional antennas intracorporeally. With a focus on antenna applications, specifics related to material optimization are excluded and focus is rather on assessing the RF conductivity performance of PEDOT:PSS:PEGDA (Section II) and its suitability for realizing antenna structures (Section III). In summary, we introduce a new fabrication method for implantable antennas, where a 3D-printer would eventually print the antenna intracorporeally via a small incision on the patient's body. This is the first time that we demonstrate feasibility of such an approach: [21] utilized inks of 9.09 S/m in conductivity, whereas we show ~$10^4$ S/m. Since this is the first time that PEDOT:PSS:PEGDA is evaluated for implanted antenna applications, we purposely select simple/standard antenna structures (dipoles and patches) in Section III to prove the concept, with no goal of antenna design optimization. The results are, of course, applicable to multiple antenna design.

## II. RF CONDUCTIVITY OF PEDOT:PSS:PEGDA

### *A. Biomaterial Composition and Formulation*

The conductive biomaterial used in this study is based on PEDOT:PSS biomaterial which is known to be biocompatible [30] and can be modified by various additives to provide desired mechanical properties [31], good conductivity [32], and printability [30]. Conductivity of the PEDOT:PSS solution (Heraeus Electronic Materials, Clevios # TM PH1000) is lower than 1 S/cm and Ethylene Glycol (EG) (Sigma Aldrich, # 324558) was used to increase its conductivity [32]. To cure the biomaterial, the photocurable PEGDA 575 (Sigma Aldrich, # 437441-500ML) with Phenylbis (2, 4, 6-trimethylbenzoyl) Phosphine Oxide (BAPO) photo initiator (IMG Resins, # 162881-26-7) was used to cure the biomaterial at room temperature. The PEDOT:PSS concentration was selected based on adequate viscosity and printability as 3-7% w/v PEDOT:PSS, 8% v/v EG, 21 or 30% v/v PEGDA, and 1% w/v PEGDA photo initiator. We examined two different PEGDA concentrations of 21% and 30% to evaluate the trade-off between conductivity and curing capabilities. To fabricate the biomaterial, the as received PEDOT:PSS was stirred for 6 hours and filtered using a 450 µm syringe filter. The filtered solution was cryogenically frozen in liquid nitrogen and lyophilized for 72 hours to eliminate the water content. To make 10 ml biomaterial with 30% PEGDA content, 350 mg of the lyophilized PEDOT:PSS was re-dispersed in a solution of 0.8 ml EG and 6.2 ml deionized water and mixed with a vortex mixer until no solid content was observed. In a separate tube, 3 ml of PEGDA was prepared and 33.6 mg BAPO photo-initiator was gradually added to the tube and mixed by vortex mixer. To make a homogenous ink, the liquid was thoroughly mixed with the vortex mixer and sonicated

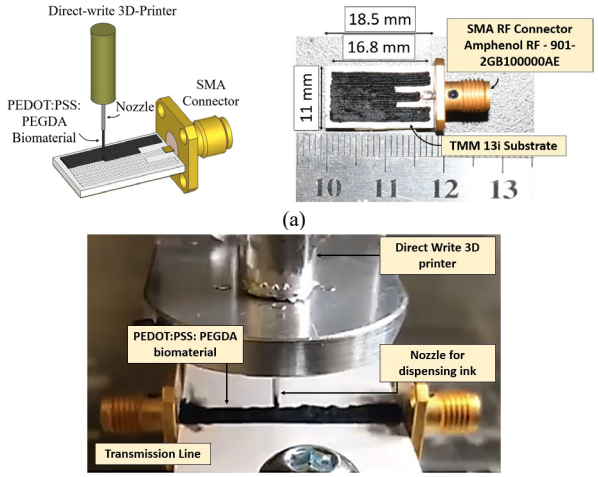


Fig. 1. Direct-write 3D printing: (a) schematic illustrating the 3D-printing process (left) and patch antenna on 1.27-mm-thick substrate (right) (b) 4.5-mm-thick transmission line on 1.52 mm substrate.

for 1 hour before being grounded with a Disposable Tissue Grinder (Fisher Scientific, # 02-542-07). According to [33], 2-3% PEGDA would yield the highest conductivity for PEDOT:PSS films. However, other research recommended using 30% PEGDA content for fast curing capability and improved mechanical properties [34]. In this paper, we have investigated the RF performance of PEDOT:PSS biomaterial with 21% and 30% PEGDA content as both show good curing capabilities and adequate conductivity at DC with the 21% ink having higher conductivity and lower curability conditions compared to the 30% one.

The prepared biomaterial was manually loaded into a 1 ml glass syringe with a nozzle diameter of 514 µm and loaded into a direct-write printer. The ink was subsequently deposited on the Printed Circuit Board (PCB) substrates with an SMA connector in either one end or two ends as to form the desired antenna or transmission line's (TL) shape as shown in Fig. 1. The nozzle distance from surface was set to 400 µm and printing tracks were separated by 400 µm to print a 2-dimensional coherent structure. The printed samples were cured by a 365 nm UV curing light (Thorlabs, # CS20K2,) with a 220 mW/cm$^2$ light intensity at a distance of 2 mm from the sample with exposure time of 1 min/cm$^2$ of the sample. A thorough analysis of the abovementioned material aspects will be reported in a future publication. Instead, we herewith focus on the RF performance of the PEDOT:PSS:PEGDA biomaterial and associated antennas.

### *B. Analyzing the Concentration-Dependent Behavior of PEDOT: PSS Biomaterial with Dipole Antennas*

In order to evaluate the PEDOT:PSS biomaterial at RF frequencies, three different concentration were examined using standard 2.4 GHz dipole antennas printed on a Polysine glass slide. A surface-mount transmission line transformer from MiniCircuits (SCTX1-83-2W+) was used as a balun. The telemetry setup involved a copper dipole

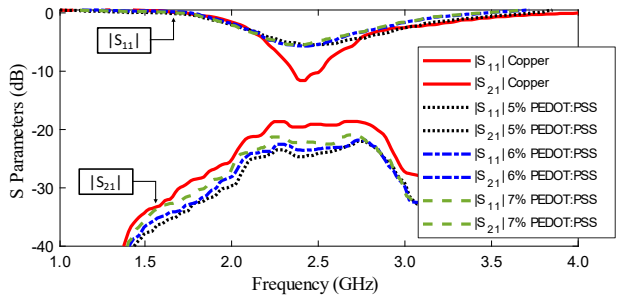


Fig. 2. Comparative performance analysis of varying concentrations of PEDOT:PSS using dipole antennas.

antenna as a reference transmitter, while dipoles with 5%, 6% and 7% PEDOT:PSS biomaterial served as receivers at 30 cm away. The reflection and transmission coefficients were measured using a network analyzer, as shown in Fig. 2. The reflection coefficient of 5%, 6% and 7% at 2.4 GHz was -3.92 dB, -5.64 dB and -5.45 dB, respectively. The transmission coefficients were -24.40 dB, -23.57 dB and -22.15 dB, respectively. That is, 7% PEDOT:PSS biomaterial performs better and is considered in the following investigations. Further material optimization can be pursued in the future.

### *C. Conductivity Measurement Results*

To determine the RF conductivity of PEDOT:PSS:PEGDA biomaterial, we pursued the transmission line (TL) approach described in [35,36]. Specifically, we: (a) fabricated two microstrip TLs of different lengths (3 and 5 cm, see inset of Fig. 3(a)), (b) measured the return loss and insertion loss, (c) used the S-parameter de-embedding technique to eliminate reflection losses at the input and output junctions, (d) removed dielectric and radiation losses by relying on copper-based counterparts of the TLs, and (e) derived the intrinsic conductivity of the printed material. All transmission lines were 4.5-mm-wide and fabricated on 1.52-mm-thick Rogers RO3003 substrate ($\varepsilon_r$=3, tan$\delta$=0.01). To realize the copper and PEDOT:PSS:PEGDA samples, we used copper tape, 21% PEGDA bio-material, and 30% PEGDA bio-material, respectively. Measurements of the reflection ($|S_{11}|$) and transmission ($|S_{21}|$) coefficient parameters for all six TLs (copper and two biomaterial concentrations, each of two different lengths) are shown in Fig. 3(a). Measurements were taken using a Keysight PNA-L N5235A network analyzer in the 10 MHz to 6 GHz range. As seen, the insertion loss of the 21% and 30% biomaterials at 1 GHz is 0.28 dB/cm and 0.31 dB/cm respectively, which is only 0.26 dB/cm and 0.29 dB/cm higher than copper. At 4 GHz, insertion loss increases to 0.81 dB/cm and 1.08 dB/cm respectively, which is only 0.68 dB/cm and 0.95 dB/cm higher than copper. These results confirm the promise of PEDOT:PSS:PEGDA as a highly conductive biomaterial. Indeed, conductivity results in Fig. 3(b) (derived using the approach in [35]) show that the average conductivity of both biomaterial concentrations is >$10^4$ S/m up to ~5 GHz which covers the bands of interest to implantable applications in Section I.

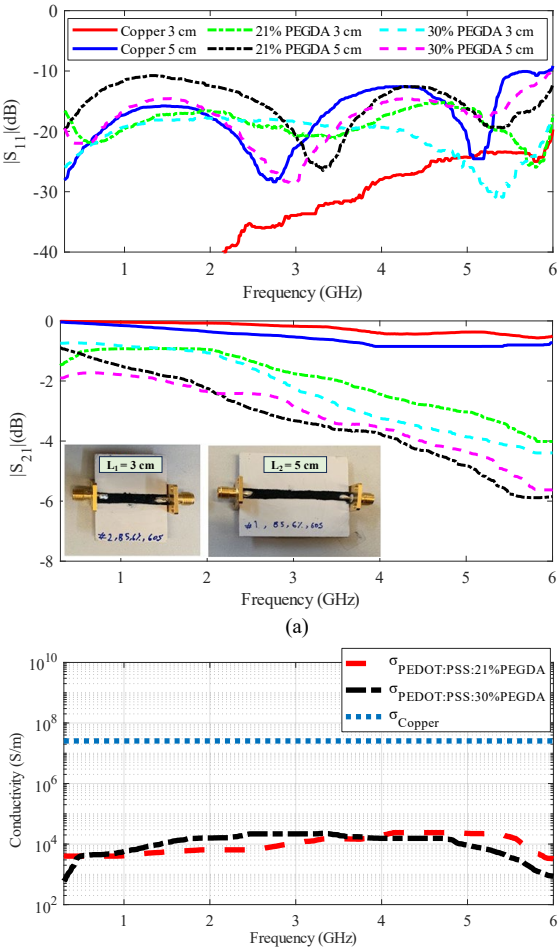


Fig. 3. (a) Measurements of the TL reflection ($|S_{11}|$) and transmission coefficient ($|S_{21}|$) (Inset shows the fabricated transmission lines), and (b) resulting conductivity ($\sigma$).

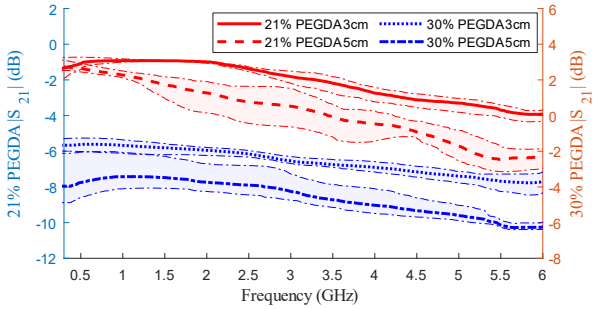


Fig. 4. Repeatability studies for 3 transmission line samples each of 21% and 30% PEGDA biomaterial.

### *D. Repeatability Assessment*

To assess repeatability, we evaluated 3 distinct samples of TLs of each length and conducted 5 tests on each sample (Fig. 4); the center line represents the average of 3 samples and the shaded region represents the largest deviation about the mean. In summary, the average deviation about the mean for 21% PEGDA content was 0.326 dB and 0.854 dB for the 3 cm and 5 cm samples, respectively. For 30% PEGDA content, the average deviation was 0.316 dB and 0.727 dB for the 3 cm and 5 cm samples, respectively. These discrepancies are mostly attributed to the weak contact between the conductive biomaterial TL and the SMA connector. By printing directly on the metal pin of the SMA connector rather than establishing a connection afterward, this inaccuracy may be minimized. Another method is to use an adhesive such as silver glue to strengthen the contact surface and establish a more durable connection.

## III. RF Antenna Performance

The performance of free-space dipole and implantable patch antennas made of PEDOT:PSS with 21% and 30% PEGDA biomaterial is hereafter assessed. Per Section I, we purposely select simple/standard antennas as we are not aiming to optimize any particular design. Accordingly, we are not aiming to overcome the reduced conductivity of PEDOT:PSS:PEGDA as compared to copper. If we want to have the ability to print intracorporeally, we are going to have to sacrifice some properties. Approaches for overcoming low conductivity issues are well established in the literature.

TABLE II
COMPARISON OF RF PARAMETERS FOR IMPLANTED PATCH ANTENNAS MADE OF COPPER AND PEDOT:PSS BIOMATERIAL

| Antenna Material | $\|S_{11}\|$ at 2.4 GHz (dB) | $\|S_{21}\|$ at 2.4 GHz (dB) | Simulated Gain (dB) | Side Lobe Level (dB) | Radiation Efficiency |
|---|---|---|---|---|---|
| Copper | -13.72 | -25.64 | -10.20 | -7.5 | 2.21% |
| PEDOT:PSS:21%PEGDA | -12.74 | -28.67 | -13.60 | -7.0 | 1.05% |
| PEDOT:PSS:30%PEGDA | -20.17 | -29.54 | -12.01 | -7.4 | 1.46% |

### *A. Simulation of Conductivity Effects on Antenna Performance*

Previous studies using reflection characteristics have indicated that a minimum conductivity of $10^4$ S/m may be suitable for implantable antenna applications [23]. Here, we expand upon the work reported in [23] to demonstrate gain results, and particularly realized gain that takes mismatch into account to determine adequate conductivity. Simulations were performed using the finite element method in the CST Microwave Studio (MWS). As a proof of concept, we investigated free-space half-wavelength dipole antennas at 403 MHz, 915 MHz, 2.4 GHz and an implanted patch antenna at 2.4 GHz. The implant antenna setup considers the 11 mm × 18.5 mm patch reported in [37], placed 5 mm deep inside a rectangular frequency-dependent 2/3 muscle tissue phantom representing average tissue properties [37]. A 2nd order Debye model was used in simulation with an 8th order fitting scheme, having an error of 13.4% before interpolation. A frequency domain solver was used to obtain the results. As mentioned in [37], the implanted antenna was directly designed inside a tissue environment and the free-space performance was not evaluated separately. Details on tissue loading effects are well reported in the literature [38,39].

Simulated maximum realized gain results as a function of conductivity is shown in Fig. 5. As seen, the gain is fairly constant above $\sigma=10^6$ S/m, below which deterioration increases. For the case of 2.4 GHz implant patch antenna, at $\sigma=10^6$ S/m, the maximum 3-D realized gain is -11.4 dB, at $\sigma=10^5$ S/m it reduces by only 0.6 dB, and at $\sigma=10^4$ S/m it reduces by 2.6 dB. Similar results were obtained for the remaining antennas. Based on these findings, we conclude that conductivities of $>10^5$ S/m are excellent, while conductivities of $\sim10^4$ S/m are adequate to fabricate antennas.

### *B. Free-Space PEDOT:PSS:PEGDA Antenna Performance*

To validate the conductivity findings of Fig. 3(b), we first tested a free-space half-wavelength dipole antenna operating at 2.4 GHz. For comparison purposes, we fabricated two antenna samples, with 21% and 30% PEGDA, respectively. Both antennas were printed on a Polysine glass slide. Reflection coefficient measurements were taken using a network analyzer, while radiation patterns were measured in the ElectroScience Laboratory anechoic chamber. The balun mentioned in section II.B was used. We also simulated these antennas in CST MWS using the conductivity values obtained in Section II. Finally, we contrasted the resulting performance vs. "gold-standard" copper.

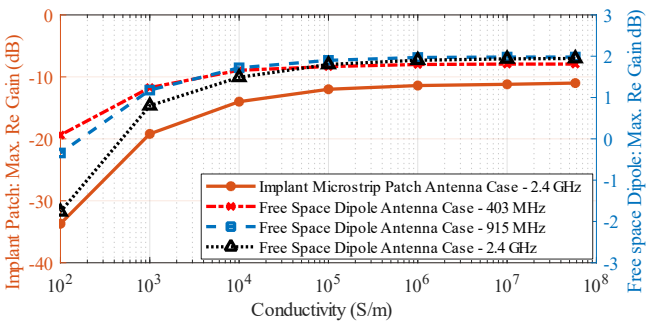


Fig. 5. Effect of varying conductivity in simulation of the max. realized gain of a implanted patch antenna and free-space half-wavelength dipole antennas.

Reflection coefficient results are summarized in Fig. 6(a), while far-field radiation patterns in the E- and H-planes are shown in Fig. 6(b). For the free space dipole antenna simulations, the complex impedance at the resonant frequency for copper is 47.13+j2.02 Ω. For PEDOT:PSS 21% and 30% PEGDA, it is 56.14-j3.49 Ω and 66.17 - j11.27 Ω, respectively. The quality (Q) factor obtained using simulation is 6.96, 6.69 and 6.49, respectively. Overall, the simulation and measurement results are in good agreement. Slight differences in performance of PEDOT:PSS:PEGDA vs. copper dipole antennas can be rectified by fine-tuning the length of the dipole legs. The smaller bandwidth observed with the PEDOT:PSS:PEGDA biomaterial as compared to copper is likely due to shrinkage in the biomaterial post-printing. In fact, the bandwidth of the 21% PEGDA biomaterial is smaller than the 30% PEGDA hinting to larger shrinkage. This shrinkage only occurs in air-based media and is not of relevance to our intended intracorporeal printing application. Further research is required to fully understand this phenomenon. Figure 6(c) illustrates the impact of fabrication errors on the $|S_{11}|$ performance. These variations can be attributed to both material and fabrication inconsistencies. Nevertheless, all samples consistently demonstrate

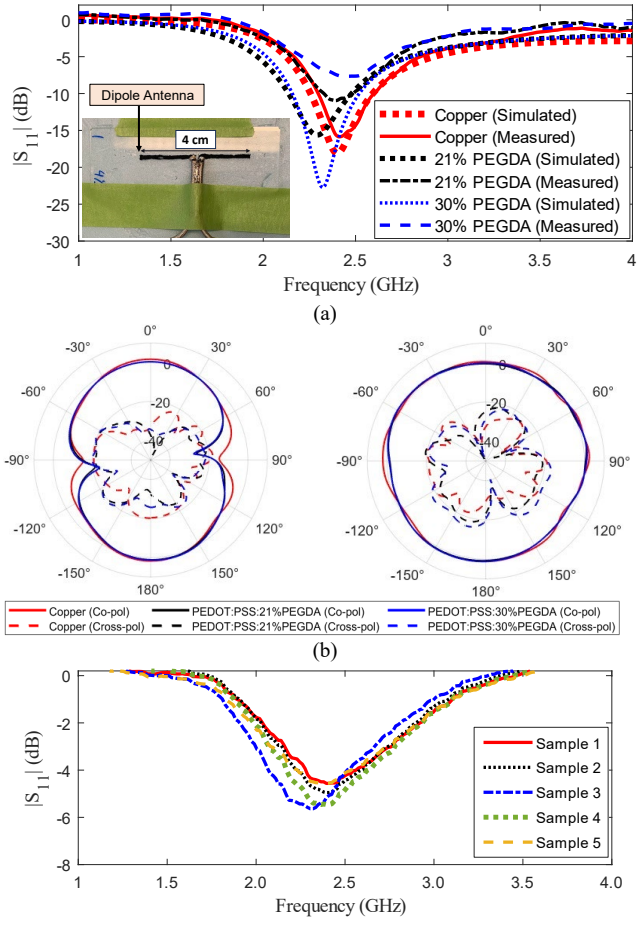


Fig. 6. Performance of copper and PEDOT:PSS:PEGDA dipole antenna at 2.4 GHz operating in free-space: (a) reflection coefficient ($|S_{11}|$) performance, (b) E-and H-plane radiation patterns, and (c) change in $|S_{11}|$ response across 5 samples of 30% PEGDA.

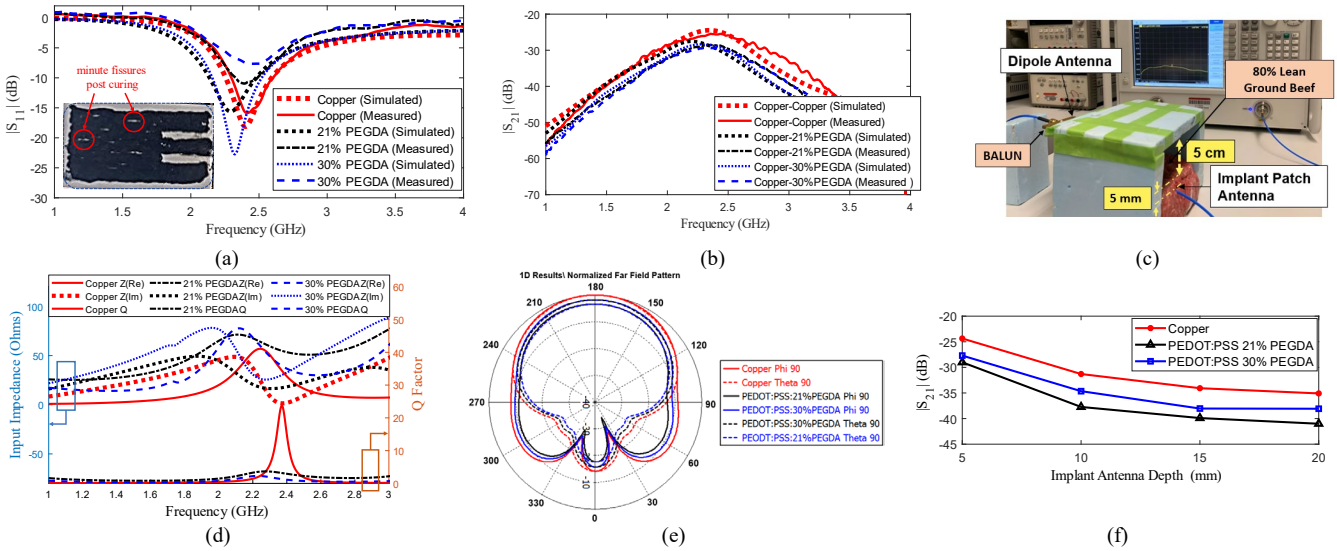


Fig. 7. Comparison of RF performance of copper and PEDOT:PSS:PEGDA implanted patch antennas in tissue media (a) reflection coefficient ($|S_{11}|$) of implanted patches, (b) transmission coefficient ($|S_{21}|$) between the implanted patches and copper dipoles. (c) telemetry setup, (d) input Impedance and Q factor. (e) simulated normalized radiation patterns, and (f) effect of implant depth on $|S_{21}|$ performance.

that the dipole resonates closely within the operational band. The maximum co-pol gain measured for the copper prototype was 1.86 dB (0.086 dB lower than the simulated value), while for 21% PEGDA and 30% PEGDA it was 1.06 dB and 0.805 dB, respectively. The combined effect of poor contact between the antenna-feed mechanism and inadequate contact during its rotation in the anechoic chamber degrades the measured gain. The cross-pol components of both PEDOT:PSS: 21% and 30% PEGDA biomaterials were below -15 dB for all scan angles. The simulation results showed that the radiation efficiency for copper was 99.10%, while PEDOT:PSS with 21% PEGDA and 30% PEGDA exhibited lower radiation efficiencies of 84.76% and 81.57% respectively.

### *C. Implantable PEDOT:PSS:PEGDA Antenna Performance*

We expand our studies by considering the 2.4 GHz microstrip implantable patch antenna of Section III.A [37]. Two prototypes were fabricated using PEDOT:PSS with 21% and 30% PEGDA content, respectively (see inset of Fig. 7(a)). They were inserted 5 mm deep inside an 80% lean / 20% fat ground beef phantom used to replicate the average human tissues [37]. A telemetry setup was then implemented (see Fig. 7(c)) where each of the implanted patches were set to communicate with a 2.4 GHz copper-based half-wavelength dipole placed 5.5 cm away.

Reflection coefficient results for the patch antennas and transmission coefficient results for the system are shown in Fig. 7(a) and 7(b) respectively. The simulated complex impedance and Q factor for copper, PEDOT:PSS 21% and 30% PEGDA are shown in Fig.7(d). For the copper-based antenna, the input impedance observed through simulation at 2.4 GHz is 28.91 + j1.98 Ω. For fabricated antennas with 21% and 30% PEGDA, the corresponding input impedances are 53.5 + j18.23 Ω and 36.67 + j32.85 Ω, respectively. Furthermore, the Q factors at 2.4 GHz are 14.98 for copper, 2.93 for 21% PEGDA, and 1.12 for 30% PEGDA. As seen, both the 21% and 30% PEGDA implanted antennas resonate at 2.4 GHz with $|S_{11}|$ being well below -10 dB. Transmission loss at 2.4 GHz with 21% PEGDA is 3.05 dB higher than the copper counterpart. With 30% PEGDA, it is 3.84 dB. The non-uniform pattern of $|S_{11}|$ for the biomaterials is mainly due to inconsistencies in fabrication. Nevertheless, the minimum $|S_{11}|$ consistently stays well below -10 dB. As a result, the power entering the antenna is well within acceptable limits, explaining the observed satisfactory agreement in the $|S_{21}|$ measurement. A zoomed-in view of the patch antenna as depicted in the inset of Fig. 7(a) reveals tiny fissures in the printed structure, as a consequence of microcracks after curing the sample. This can be eliminated by using smaller diameter nozzles and reducing the spacing between printing tracks for more compact printing, thus improving the antenna performance. Moreover, any frequency shifts induced by reduced conductivity can be mitigated through careful adjustment of the antenna's geometry. Increasing the size of the ground plane can also lead to improvements in gain and reductions in the side lobe levels. Simulated radiation patterns (normalized) are shown in Fig. 7(e). Table II provides a detailed comparison of the RF performance between the implanted patch antenna using the PEDOT:PSS:PEGDA biomaterial and copper. It presents a comprehensive analysis of various parameters, highlighting the performance differences using lower conductivity biomaterial. The lower gain observed in the case of 21% PEGDA can be attributed to the conductivity values considered in CST, as obtained in Section II.C. Note that CST uses a fitting scheme with an error of 13.4% before interpolation. Measured results, however, indicate a better performance. To characterize the communication link, the implantable antenna depth was varied from 5 mm to 20 mm and the performance is compared in Fig. 7(f). Other communication link parameters can be calculated based on previously reported approaches [40, 41]. SAR simulations were also conducted considering a 1010 kg/m$^3$ tissue mass density [41]. To comply with the Federal Communications Commission (FCC) guidelines of $SAR_{1g}$<1.6 W/kg, the maximum input power was found to be 9.9 dBm, 14.1 dBm and 11.7 dBm, for implanted patches based on copper, 21% PEGDA and 30% PEGDA, respectively.

## IV. Conclusion

This paper investigated the feasibility of PEDOT:PSS:PEGDA biomaterial in fabricating RF structures (transmission lines and antennas) using 3D-printing with a robotic probe, with an emphasis on examining the impact of decreased conductivity on RF performance. The vision is for this approach to ultimately 3D-print wireless implants intracorporeally via a minor incision on the patient's body. Our studies showed that the biomaterial containing 7% PEDOT:PSS demonstrates superior performance compared to those with 5% and 6% content. Meanwhile, compositions with 21% and 30% PEGDA exhibit a conductivity of approximately $10^4$ S/m up to 5 GHz. Simulations confirmed these conductivity values to be appropriate for implantable antenna applications. Comparing the two, 21% PEGDA content exhibits poorer curing properties, while 30% PEGDA exhibits slightly lower conductivity. Compared to gold standard copper,

PEDOT:PSS:21% PEGDA exhibited only 0.8 dB lower measured maximum 3-D gain in free space and 3.05 dB lower measured transmission coefficient for an implantable scenario. PEDOT:PSS:30% PEGDA exhibited 1 dB lower measured 3-D gain in free space and 3.84 dB lower measured transmission coefficient for an implantable scenario. To counter lower gain values, a standard technique to increase antenna footprint could be implemented: since the printing process is now minimally invasive, miniaturization requirements can be relaxed. Future research will focus on optimizing the biomaterial at RF frequencies, performing parametric studies on the effects of manufacturing defects on the antenna performance, and printing of both dielectrics and PEDOT:PSS:PEGDA inks inside biological tissue media for various diagnostic, therapeutic, and monitoring applications.

## REFERENCES


[1] C. Plummer, "The use of permanent pacemakers in the detection of cardiac arrhythmias," *Europace*, vol. 3, no. 3, pp. 229–232, 2001.

[2] D. Wessels, "Implantable pacemakers and defibrillators: device overview & EMI considerations," *2002 IEEE International Symposium on EM Compatibility*, Minneapolis, MN, USA, 2002, pp. 911-915 vol.2.

[3] A. Kiourti and K. S. Nikita, "A Review of In-Body Biotelemetry Devices: Implantables, Ingestibles, and Injectables," in *IEEE Transactions on Biomedical Engineering*, vol. 64, no. 7, pp. 1422-1430, July 2017

[4] M. Smith, "Monitoring intracranial pressure in traumatic brain injury," *Anesthesia & Analgesia*, vol. 106, no. 1, pp. 240–248, 2008.

[5] P. Limousin *et al.*, "Electrical stimulation of the subthalamic nucleus in Advanced Parkinson's Disease," *New England Journal of Medicine*, vol. 339, no. 16, pp. 1105–1111, 1998.

[6] W. M. M. Schuepbach *et al.*, "Neurostimulation for parkinson's disease with early motor complications," *New England Journal of Medicine*, vol. 368, no. 7, pp. 610–622, 2013.

[7] A. L. Benabid, S. Chabardes, J. Mitrofanis, and P. Pollak, "Deep brain stimulation of the subthalamic nucleus for the treatment of parkinson's disease," *The Lancet Neurology*, vol. 8, no. 1, pp. 67–81, 2009.

[8] D. Lu *et al.*, "Bioresorbable, wireless, passive sensors as temporary implants for monitoring regional body temperature," *Advanced Healthcare Materials*, vol. 9, no. 16, p. 2000942, 2020.

[9] S. Rao *et al*., "Wireless gastric stimulators," *Texas Symposium on Wireless and Microwave Circuits and Systems*, Waco, TX, USA, 2014, pp. 1-4.

[10] J. Y. Lucisano, T. L. Routh, J. T. Lin and D. A. Gough, "Glucose Monitoring in Individuals With Diabetes Using a Long-Term Implanted Sensor/Telemetry System and Model," in *IEEE Transactions on Biomedical Engineering*, vol. 64, no. 9, pp. 1982-1993, Sept. 2017.

[11] F. Boscari *et al.*, "Implantable and transcutaneous continuous glucose monitoring system: A randomized cross over trial comparing accuracy, efficacy and acceptance," *Journal of Endocrinological Investigation*, vol. 45, no. 1, pp. 115–124, 2021.

[12] J. M. Schierholz and J. Beuth, "Implant infections: A haven for opportunistic bacteria," *Journal of Hospital Infection*, vol. 49, no. 2, pp. 87–93, 2001.

[13] P. S. Barie and S. R. Eachempati, "Surgical site infections," *Surgical Clinics of North America*, vol. 85, no. 6, pp. 1115–1135, 2005.

[14] M. Ribeiro, *et al*, "Infection of orthopedic implants with emphasis on bacterial adhesion process and techniques used in studying bacterial-material interactions," *Biomatter*, vol. 2, no. 4, pp. 176–194, 2012.

[15] X. Li *et al*, "The injectable neurostimulator: An emerging therapeutic device," *Trends in Biotechnology*, vol. 33, no. 7, pp. 388–394, 2015.

[16] A. Kiourti and K. S. Nikita, "A Review of Implantable Patch Antennas for Biomedical Telemetry: Challenges and Solutions [Wireless Corner]," in *IEEE Antennas and Propagation Magazine,* vol. 54, no. 3, pp. 210-228, June 2012.

[17] A. Garcia-Miquel *et* al, "Miniaturization effects on implantable antennas for biomedical applications," *2015 9th European Conference on Antennas and Propagation,* 2015, pp. 1-4.

[18] A. Kiourti *et al*., "Next-Generation Healthcare: Enabling Technologies for Emerging Bioelectromagnetics Applications," in *IEEE Open Journal of Antennas and Propagation*, vol. 3, pp. 363-390, 2022.

[19] A. Kiourti and K. S. Nikita, "Miniaturization vs gain and safety considerations of implantable antennas for wireless biotelemetry," *Proceedings of the 2012 IEEE International Symposium on Antennas and Propagation*, 2012, pp. 1-2.

[20] A. Simeunović, K. Wolf, K. Tierling and D. J. Hoelzle, "A Surgical Robot for Intracorporeal Additive Manufacturing of Tissue Engineering Constructs," in *IEEE Robotics and Automation Letters*, vol. 7, no. 3, pp. 7495-7502, July 2022.

[21] K. Hall, H. Zhang and C. Furse, "Design of an Interstitial Microwave Applicator for 3D Printing in the Body," in *IEEE Journal of Electromagnetics, RF and Microwaves in Medicine and Biology*, vol. 4, no. 4, pp. 260-264, Dec. 2020.

[22] A. A. Adib *et al.*, "Direct-write 3D printing and characterization of a gelma-based biomaterial for intracorporeal tissue engineering," *Biofabrication*, vol. 12, no. 4, p. 045006, 2020.

[23] F. Curry *et al.*, "Biostable conductive nanocomposite for implantable subdermal antenna," *APL Materials*, vol. 8, no. 10, p. 101112, 2020.

[24] Federal Communications Commission | The United States of America. Available at: https://transition.fcc.gov/oet/spectrum/table/fcctable.pdf (Accessed: February 14, 2023).

[25] D. Khodagholy *et al*., "In vivo recordings of brain activity using organic transistors," in *Nature Communications,* vol. 4, no. 1, 2013.

[26] A. I. Hofmann *et al.*, "All-polymer conducting fibers and 3D prints via melt processing and templated polymerization," *ACS Applied Materials & Interfaces*, vol. 12, no. 7, pp. 8713–8721, 2020.

[27] G. de la Osa *et al*, "Printing of graphene nanoplatelets into highly electrically conductive three-dimensional porous macrostructures," *Chemistry of Materials*, vol. 28, no. 17, pp. 6321–6328, 2016

[28] K. Prashantha and F. Roger, "Multifunctional Properties of 3D printed poly(lactic acid)/graphene nanocomposites by fused deposition modeling," *Journal of Macromolecular Science*, Part A, vol. 54, no. 1, pp. 24–29, 2016.

[29] M. Wajahat *et al*., "3D printing of FE3O4 functionalized graphene-polymer (FGP) composite microarchitectures," *Carbon*, vol. 167, pp. 278–284, 2020. doi:10.1016/j.carbon.2020.05.045

[30] M. Asplund *et al.*, "Toxicity evaluation of PEDOT/biomolecular composites intended for neural communication electrodes," *Biomedical Materials*, vol. 4, no. 4, p. 045009, 2009.

[31] H. Yuk *et al*., "3D printing of conducting polymers," *Nature Communications*, vol. 11, no. 1, 2020.

[32] H. Yan, T. Jo, and H. Okuzaki, "Highly conductive and transparent poly(3,4-ethylenedioxythiophene)/poly(4-styrenesulfonate) (PEDOT/PSS) thin films," *Polymer Journal*, vol. 41, no. 12, pp. 1028–1029, 2009.

[33] D. Alemu Mengistie, P.-C. Wang, and C.-W. Chu, "Effect of molecular weight of additives on the conductivity of PEDOT:PSS and efficiency for ITO-Free Organic Solar Cells," *Journal of Materials Chemistry A*, vol. 1, no. 34, p. 9907, 2013.

[34] J. Huang, Z *et al.*, "Thermally assisted 3D printing of bio-polymer with high solute loading with improved mechanical properties," *Additive Manufacturing*, vol. 59, p. 103088, 2022.

[35] Z. Wang, "Electronic Textile Antennas and Radio Frequency Circuits for Body-Worn Applications." Doctoral dissertation, Electrical and Computer Engineering, Ohio State University, USA, 2014. [Online] Available: http://rave.ohiolink.edu/etdc/view?acc_num=osu1396955748.

[36] D. Pozar, *Microwave Engineering*. John Wiley & Sons Inc, Feb. 2004.

[37] J. Blauert and A. Kiourti, "Bio-Matched Horn: A Novel 1–9 GHz On-Body Antenna for Low-Loss Biomedical Telemetry With Implants," in *IEEE Transactions on Antennas and Propagation*, vol. 67, no. 8, pp. 5054-5062, Aug. 2019.

[38] A. Kiourti and K. S. Nikita, "Numerical assessment of the performance of a scalp-implantable antenna: Effects of head anatomy and dielectric parameters," Bioelectromagnetics, vol. 34, no. 3, pp. 167–179, 2012.

[39] D. Nikolayev, M. Zhadobov and R. Sauleau, "Impact of Tissue Electromagnetic Properties on Radiation Performance of In-Body Antennas," in IEEE Antennas and Wireless Propagation Letters, vol. 17, no. 8, pp. 1440-1444, Aug. 2018

[40] M. Manoufali, *et al*, "In Situ Near-Field Path Loss and Data Communication Link for Brain Implantable Medical Devices Using Software-Defined Radio," in IEEE Transactions on Antennas and Propagation, vol. 68, no. 9, pp. 6787-6799, Sept. 2020

[41] J. Kim and Y. Rahmat-Samii, "Implanted antennas inside a human body: Simulations designs and characterizations", in *IEEE Trans. Microw. Theory Techn*., vol. 52, no. 8, pp. 1934-1943, Aug. 2004.